High Precision Measurement of Compton Scattering in the 5 GeV region

P. Ambrozewicz,[1] L. Ye,[2] Y. Prok,[3] I. Larin,[4] L. Gan,[5] A. Gasparian,[1] S. Kowalski,[3] D. Dutta,[2] Z. Ahmed,[1] A. Ahmidouch,[1] K. Baker,[6] V. Baturin,[7] L. Benton,[1] A. Bernstein,[3] V. Burkert,[7] E. Clinton,[8] P. Cole,[9] P. Collins,[10] D. Dale,[9] S. Danagoulian,[1] G. Davidenko,[4] R. Demirchyan,[1] A. Deur,[7] A. Dolgolenko,[4] G. Dzyubenko,[4] R. Ent,[7] G. Fedotov,[11] J. Feng,[5] M. Gabrielyan,[12] H. Gao,[13] N. Gevorkyan,[14] S. Gevorkyan,[15] A. Glamazdin,[16] V. Goryachev,[4] L. Guo,[17] V. Gyurjyan,[7] K. Hardy,[1] J. He,[18] E. Isupov,[11] M. Ito,[7] L. Jiang,[5] H. Kang,[19] O. Kasinov,[9] D. Kashy,[7] M. Khandaker,[20] P. Kingsberry,[20] F. Klein,[21] A. Kolarkar,[12] M. Konchatnyi,[22] O. Korchin,[22] W. Korsch,[12] O. Kosinov,[9] M. Kubantsev,[23] A. Kubarovskiy,[7] V. Kubarovsky,[7] D. Lawrence,[7] X. Li,[5] M. Levillain,[1] H. Lu,[24] L. Ma,[5] P. Martel,[8] V. Matveev,[4] D. McNulty,[3] B. Mecking,[7] A. Micherdzinska,[25] B. Milbrath,[26] R. Minhart,[27] R. Miskimen,[8] V. Mochalov,[28] B. Morrison,[10] S. Mtingwa,[1] I. Nakagawa,[12] S. Overby,[1] E. Pasyuk,[10] M. Payen,[1] K. Park,[7] R Pedroni,[1] W. Phelps,[29] D. Protopopescu,[30] D. Rimal,[17] B. Ritchie,[10] T. Rodrigues,[31] C Salgado,[20] A. Shahinyan,[14] A Sitnikov,[4] D. Sober,[21] S. Stepanyan,[7] W. Stephens,[27] S. Taylor,[7] A. Teymurazyan,[12] J. Underwood,[1] A. Vasiliev,[32] V. Vishnyakov,[4] D. P. Weygand,[7] M. Wood,[8] Y. Zhang,[13] S. Zhou,[33] and B. Zihlmann[7]

[1]North Carolina A&T State University, Greensboro, NC 27411, USA
[2]Mississippi State University, Mississippi State, MS 39762, USA
[3]Massachusetts Institute of Technology, Cambridge, MA 02139, USA
[4]Alikhanov Institute for Theoretical and Experimental Physics, Moscow 117218, Russia
[5]University of North Carolina Wilmington, Wilmington, NC 28403, USA
[6]Hampton university, Hampton, VA 23606, USA
[7]Thomas Jefferson National Accelerator Facility, Newport News, VA 23606, USA
[8]University of Massachusetts, Amherst, MA 01003, USA
[9]Idaho State University, Pocatello, ID 83209, USA
[10]Arizona State University, Tempe, AZ 85281, USA
[11]Moscow State University, Moscow 119991, Russia
[12]University of Kentucky, Lexington, KY 40506, USA
[13]Duke University and Triangle University Nuclear Lab, Durham, MC 27708, USA
[14]Yerevan Physics Institute, Yerevan 0036, Armenia
[15]Joint Institute for Nuclear Research, Dubna 141980, Russia,
On leave of absence from Yerevan Physics Institute, Yerevan, Armenia
[16]Kharkov Institute of Physics and Technology, Kharkov, 310108, Ukraine
[17]Florida International University, Miami, FL 33199, USA
[18]Institute of High Energy Physics, Chinese Academy of Sciences, Beijing 100049, China
[19]Seoul National University, Seoul 08826, Korea
[20]Norfolk State University, Norfolk, VA 23504, USA
[21]The Catholic University of America, Washington, DC 20064, USA
[22]Kharkov Institute of Physics and Technology, Kharkov 310108, Ukraine
[23]Northwestern University, Evanston, IL 60208, USA
[24]Carnegie Mellon University, Pittsburgh, PA 15213, USA
[25]George Washington University, Washington, DC 20064, USA
[26]Pacific Northwest National Laboratory, Richland, WA 99354, USA
[27]University of Virginia, Charlottesville, VA 22094, USA
[28]Institute for High Energy Physics, Protvino, 142280, Russia
[29]Christopher Newport University, Newport News, VA 23606, USA
[30]Glasgow University, Glasgow G12 8QQ, UK
[31]University of São Paulo, São Paulo 03178-200, Brazil
[32]Institute for High Energy Physics, Protvino 142280, Russia
[33]Chinese Institute of Atomic Energy, Beijing 102413, China

(Dated: December 11, 2018)

The cross section of atomic electron Compton scattering $\gamma + e \rightarrow \gamma' + e'$ was measured in the 4.40–5.45 GeV photon beam energy region by the *PrimEx* collaboration at Jefferson Lab with an unprecedented accuracy. The results are consistent with theoretical predictions that include next-to-leading order radiative corrections. The measurements provide the first high precision test of this elementary QED process at beam energies greater than 0.1 GeV.

PACS numbers: 11.80.La, 13.60.Le, 25.20.Lj

I. INTRODUCTION

Quantum-electrodynamics (QED) is considered to be one of the most successful theories in modern physics; and the Compton scattering of photons by free electrons $\gamma + e \rightarrow \gamma' + e'$ is the simplest and the most elementary pure QED process. The lowest order Compton scattering diagrams (see Fig. 1) were first calculated by Klein and Nishina in 1929 [1], and by Tamm in 1930 [2]. Higher order contributions arising from the interference between the leading order single Compton scattering amplitude and the radiative and double Compton scattering amplitudes were calculated in the 1950's [3]-[4]. Figure 2 shows the Feynman diagrams illustrating these two processes. They were subsequently re-evaluated in the 60's and early 70's to make them convenient to calculate using modern computational techniques [5]-[11]. Corrections to the leading order Compton total cross section at the level of a few percent are predicted for beam energies above 0.1 GeV [6], hence the next-to-leading order (NLO) corrections are important when studying Compton scattering at these energies.

Experiments performed so far were mostly in the energy region below 0.1 GeV ; a few experiments probed the 0.1-1.0 GeV energy range with a precision of 10–15% [12]-[15]. Only one experiment [16] measured the Compton scattering total cross section up to 5.0 GeV using a bubble-chamber detection technique. The experimental uncertainties for energies above 1 GeV were at the level of 20–70%. Due to the lack of precise data, higher order corrections to the Klein-Nishina formula have never been tested experimentally. This paper reports on new measurements of the Compton scattering cross section with a precision of 1.7% performed by the *PrimEx* collaboration at Jefferson Lab (JLab) for two separate running periods. The total cross sections for forward angles up to 2^o on ^{12}C and ^{28}Si targets were measured in the 4.40–5.45 GeV energy region. The precision achieved by this experiment provides, for the first time, an important test of the QED prediction for the Compton scattering process with corrections to the order of $\mathcal{O}(\alpha)$, where α is the fine structure constant. In this article, we will summarize the theoretical calculations (Sec. II), describe our experimental procedure (Sec. III), and present the results of the comparison between the data and the theoretical predictions (Sec. IV).

II. A SUMMARY OF THEORETICAL CALCULATIONS

The leading order Compton scattering cross sections (see Fig. 1) was first calculated by Klein and Nishina [1] and is known as the Klein-Nishina formula [17]:

$$\frac{d\sigma}{d\Omega} = \frac{r_e^2}{2}\frac{1}{[1+\gamma(1-\cos\theta)]^2}[1+\cos^2\theta + \frac{\gamma^2(1-\cos\theta)^2}{1+\gamma(1-\cos\theta)}]$$

where r_e is the classical electron radius, γ is the ratio of the photon beam energy to the rest energy of electron, and θ is the photon scattering angle. This formula predicts that the Compton scattering at high energies has two basic features: (i) the total cross section decreases with increasing beam energy, E, as approximately $1/E$, and (ii) the differential cross section is sharply peaked at small angles relative to the incident photons.

The theoretical foundation for the next-to-leading order radiative corrections to the Klein-Nishina formula had been well established by early 70's. The radiative corrections to $\mathcal{O}(\alpha)$ were initially evaluated by Brown and Feynman [3] in 1952. This correction is caused by two types of processes. The first type, a virtual-photon correction, arises from the possibility that the electron may emit and reabsorb a virtual photon in the scattering process (see left panel of Fig. 2). The second type is a soft-photon double Compton effect, in which the energy of one of the emitted photons is much smaller than the electron mass ($\omega_2 < \omega_{2max} \ll m_e$, where ω_2 is the energy of the additional photon, ω_{2max} is a cut-off energy, and m_e in the electron mass), as shown in the right panel of Fig. 2. These two contributions must be taken into account together since it is impossible to separate them experimentally. Moreover, the infrared divergence term from the virtual-photon process is canceled by the infrared divergence term in the soft-photon double Compton process, resulting in a finite physically meaningful correction (δ^{SV}). The value of δ^{SV}, where SV stands for S(oft) and V(irtual), is predicted to be negative as described by Eq. (2.6) and Eq. (2.15) in [6].

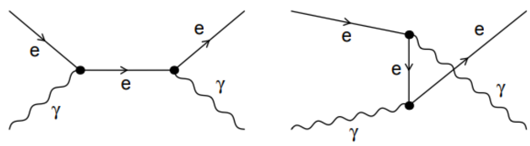

FIG. 1: The lowest-order Feynman diagrams for single Compton scattering.

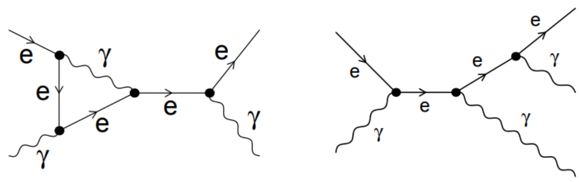

FIG. 2: Typical radiative correction (Left), and double Compton scattering contributions (Right) to single Compton scattering.

On the other hand, a hard-photon double Compton effect occurs when both emitted photons in the double Compton process have energies larger than the cut-off energy, ω_{2max}. When comparing the experimental result with the theoretical calculation, one must also take into account the contributions from the hard-photon double Compton effect since the experimental apparatus has finite resolutions leading to limitations on the measurements of both energies and angles [6]. The differential cross section of the double Compton effect was initially calculated by Mandl and Skyrme [4], and the total cross section of the Hard-photon Double Compton process (δ^{HD}) is described by Eq. (6.6) in reference [6] [1] and its value is predicted to be positive. Summing up δ^{SV} and δ^{HD}, the total NLO correction to the total cross section is predicted to be a few percent for photon beam energies up to 10 GeV.

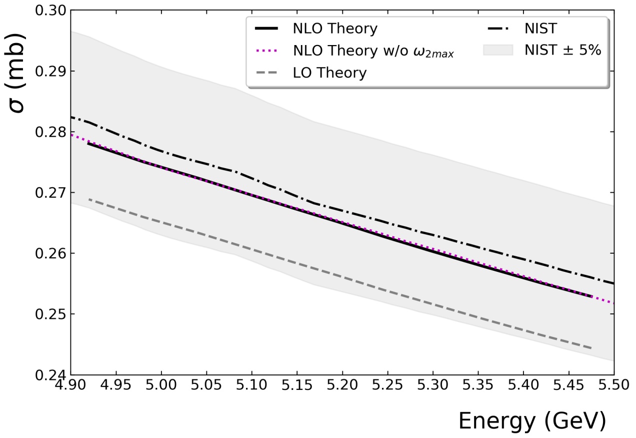

FIG. 3: Comparison of theoretical calculations of total Compton cross section using different approaches. The solid and the dotted curves are calculated by two different numerical methods - described in the text. The dotted-dashed line represents the *NIST* calculation - XCOM code. The dashed curve is calculated using the Klein-Nishina formula

In order to interpret the experimental results and compare with the theoretical predictions, one needs to develop a reliable numerical method to integrate the cross section and calculate the radiative corrections incorporating the experimental resolutions. The latter is critical in calculating the contribution from the hard photon double Compton effect correctly. As discussed above, the corrections are divided into two types (δ^{SV} and δ^{HD}) depending on whether the energy of the secondary emitted photon is less or greater than an arbitrary energy scale, denoted by ω_{2max}, which should be much smaller than the electron mass [6]. Since the physically measurable cross section contains the corrections from both types, the final integrated total cross section must be independent of the values of ω_{2max}. Two independent methods had been developed to prove this independence.

The first method [7] is based on the BASES/SPRING Monte Carlo simulation package [8]. BASES uses the stratified sampling method to integrate the differential cross section, and SPRING uses the probability information obtained during the BASES integration to generate Compton events. The parameter ω_{2max} does not enter the differential cross section explicitly but is contained in the limits of integration over the energy. For a consistency check, the total cross section was calculated with several values of ω_{2max}. While the calculated total Klein-Nishina cross section corrected with the virtual and soft photon processes (σ_{SV}) as well as the total hard photon double Compton cross section (σ_{HD}), both, depend on the ω_{2max} parameter, the sum of the two corrections ($\sigma_{SV} + \sigma_{HD}$) is independent, within 0.1%, of the choice of ω_{2max}, as expected.

The second numerical method was developed by M. Konchatnyi [9], where the parameter ω_{2max} is analytically removed from the integration. The total Compton cross section on ^{12}C with radiative corrections calculated using both numerical methods [7] [9] are compared with each other in Fig. 3. Our calculated results were also compared to the values obtained from the XCOM data base of the National Institute of Standards and Technology (*NIST*). They are in good agreement within 0.5%. Figure 3 also shows that the higher order corrections to the leading-order Klein-Nishina formula are about 4% for the beam energy in the 5 GeV region. In the data analysis described below, the BASES/SPRING method is used to calculate the radiatively corrected cross section and to generate events for the experimental acceptance study.

III. EXPERIMENTAL PROCEDURE

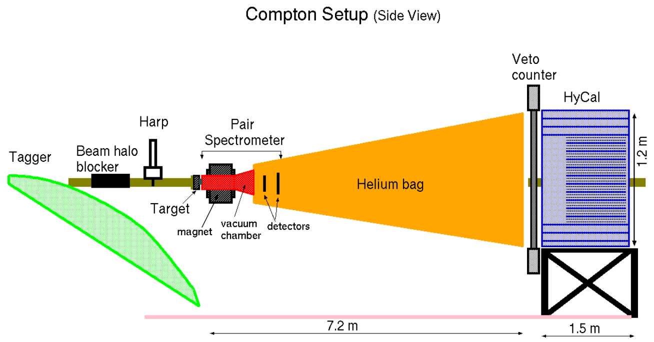

FIG. 4: Diagram, not to scale, of the experimental setup. The pair spectrometer placed between the target and the helium bag, was turned off during the Compton experiment.

The atomic electron Compton scattering process $\gamma + e \to \gamma' + e'$ was measured using the apparatus built for the *PrimEx* experiment, which aimed to measure the π^0 lifetime and was performed over two run periods in 2004 and 2010, in Hall B at JLab. The Compton scattering data were collected periodically, once per week during both running periods. The primary experimental equipment included (see Fig. 4): (i) the existing Hall B high intensity and high resolution photon tagger, which provides the timing and energy information of incident photons up to 6 GeV; (ii) solid production targets [10]: ^{12}C (5% radiation length), used during the first running period, and ^{12}C (8% radiation length) and ^{28}Si (10% radiation length) added in the second running period; (iii) a pair spectrometer (PS), located downstream of the production target, to continuously measure the relative photon tagging ratio, and consequently the absolute photon flux, which was obtained by normalizing to the absolute photon tagging efficiency measured periodically with a total absorption counter (TAC) at low beam intensities; (iv) a 118×118 cm^2 high resolution hybrid calorimeter (HyCal) with 12 scintillator charge particle veto counters, which was located ~7 m downstream of

[1] Worth noticing is that a factor of 1/4 is missing in this equation

the target, to detect forward scattered electromagnetic particles; and (v) a scintillator fiber based photon beam profile and position detector located behind HyCal for on-line beam position monitoring.

To minimize the photon conversion and electron multiple scattering, the gap between the PS magnet and the HyCal was occupied by a plastic foil container filled with helium at atmospheric pressure. The energies and positions of the scattered photon and electron were measured by the HyCal calorimeter. In conjunction with the beam energy (4.9-5.5 GeV during the first experiment and 4.4-5.3 GeV during the second one), which was determined by the photon tagger, the complete kinematics of the Compton events was determined. During the Compton runs the experimental setup was identical to the one used for the π^0 production runs, except for the pair spectrometer magnet being turned off to allow detection of both photons and electrons in the calorimeter. The use of the same experimental apparatus, as well as the similar kinematics allowed the measurement of the Compton cross section to be employed as a tool to verify the systematic uncertainty of the π^0 experiments.

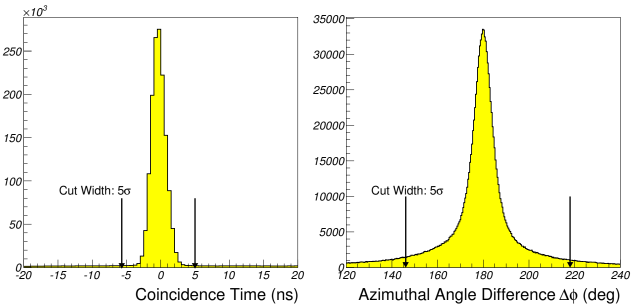

FIG. 5: (Left) The time difference between the incident photon measured by the photon Tagger and the scattered particles (photon and electron) detected by the HyCal calorimeter; (Right) Difference of the photon and the electron azimuthal angles (coplanarity). The distribution in plots on both panels still contain backgrounds.

A coincidence between the photon tagger in the energy interval of 4.4–5.5 GeV and the HyCal calorimeter with a total energy deposition greater than 2.5 GeV formed an event trigger. Only the experimental result from the higher beam energy (4.4–5.49 GeV) is presented in this report. The event selection criteria were: (i) the time difference between the incident photon, $\mathrm{t_{Tag}}$ and the scattered particles (photon and electron) detected by the HyCal calorimeter, $\mathrm{t_{HyCal}}$ had to be $|\mathrm{t_{Tag}} - \mathrm{t_{HyCal}}| < 5\sigma_\mathrm{t}$, where σ_t =1.03 ns is the timing resolution of the detector system, as shown in the left plot of Fig. 5; (ii) the difference in the azimuthal angle between the scattered photon and electron had to be $|\Delta\phi| < 5\sigma_\phi$, where $\sigma_\phi = 7^\circ$ is the azimuthal angular resolution for the first running period, as shown in the right plot of Fig. 5 (for the second running period a target dependent resolution of $\sigma_\phi = 4$ - 4.7° was used); (iii) the reconstructed reaction vertex position was required to be consistent with the target thickness and position, and the scattered particles were required to be detected within the fiducial acceptance of the HyCal calorimeter; (iv) the spatial distance between the scattered photon and electron as detected by the HyCal calorimeter had to be larger than a photon energy dependent minimum separation resulting from the reaction being elastic; the minimum separation of 16 cm for the first running period and $R_{min}(E)$ =19.0 - 1.95×(4.85-E) for the second running period; and (v) the difference between the incident photon energy as measured by the tagger, $\mathrm{E_{Tag}}$ and the reconstructed incident photon energy, $\mathrm{E_{HyCal}}$, had to be $|\mathrm{E_{Tag}} - \mathrm{E_{HyCal}}| <1$ (0.4) GeV for the first (second) running period. In the event reconstruction, the measured energy of the more energetic scattered particles (photon or electron) and the coordinate information of both scattered particles detected by the calorimeter were used. The offline energy detection threshold per particle in the HyCal calorimeter was 0.5 GeV.

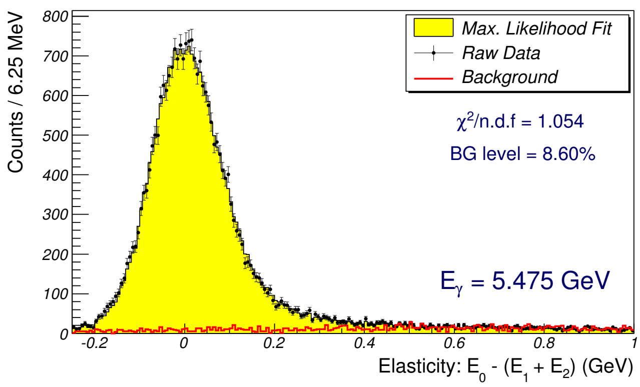

FIG. 6: An example of the yield fit, with background shown in red, for the highest energy bin.

To extract the Compton yields, the signal and background events (∼1% of the yield) were separated for every incident photon energy bin. The background originating from the target ladder and housing was determined using data from dedicated empty target runs, and the yields from these runs were normalized and subtracted away. The remaining events that passed all of the five selection criteria described above were used to form an elasticity distribution, $\Delta E = E_0 - (E_{\gamma'} + E_{e'})$, where $E_{\gamma'}$ and $E_{e'}$ are the scattered photon and electron energies, which were either measured (the first experiment) or calculated, using the Compton scattering kinematics, (the second experiment), and E_0 is the measured energy of the incident photon. The elasticity distribution was then fit to the simulated signal and background distributions, using a maximum likelihood method [18]. Their overall amplitudes were parameters in the fit, as shown in Fig. 6.

The signal was generated by a Monte Carlo simulation employing the BASES/SPRING package as described in Sec. II [7][8], which included the radiative processes and the double Compton contribution. The simulated signal events were propagated through a *GEANT*-based simulation of the experimental apparatus and then processed using the same event reconstruction software that was used to extract the experimental yield. The shape of the background was modeled by the accidental events alone for the first running period, while the pair production channel was also included for the second running period. The accidental background was selected from the data using the events that were outside the coincidence time criterion, from $|t_{\mathrm{Tag}} - t_{\mathrm{HyCal}}| > 5\sigma_t$, but satisfied the remaining four criteria described above. The pair production contribution was generated using the *GEANT* simulation toolkit with its results handled in the same manner as the experimental yield. The amplitude from the maximum likelihood fit was then used to subtract the background from the experimental yield for each incident photon energy bin, giving the Compton yield.

V. RESULTS

The Compton scattering total cross sections were obtained by combining the extracted Compton yields with the luminosity and detector acceptance. Figures 7 and 8 show the total Compton scattering cross sections from the first and the second running period, respectively. The extracted cross sections are compared to a next-to-leading order calculation for both running periods. All the results agree with the theoretical calculations within the experimental uncertainties.

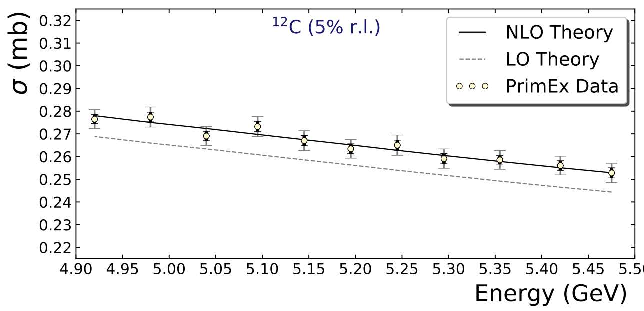

FIG. 7: The results of Compton total cross section on a ^{12}C target for the first running period. The dashed curve is calculated by using the Klein-Nishina formula. The solid curve is the result of next-to-leading order calculation. The statistical and systematic errors are shown with small and large error bars, respectively.

The average total systematic uncertainty for each data point is 1.5% for the first running period and is 1.22 - 1.79% for the second running period depending on the target (lowest for the 5% ^{12}C target and highest for the 10% ^{28}Si target). The breakdown of the uncertainties is summarized in Table I. The uncertainty in the photon flux is the largest source of uncertainty. It was determined from the long term overall stability of the beam, data acquisition live time, and tagger false count rate. The other two largest contributors to the systematic uncertainty are background subtraction and the geometrical acceptance. The uncertainty due to background subtraction was estimated from the variation in the fitting uncertainty with changes to the shape of the background

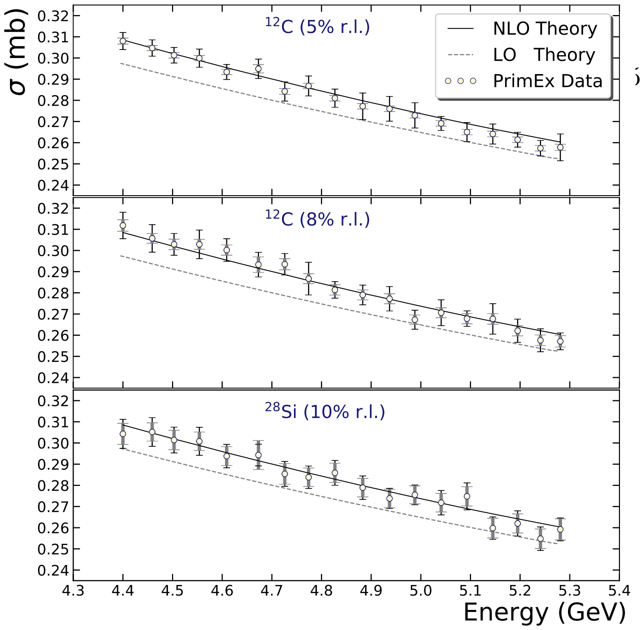

FIG. 8: The results of Compton total cross section on the two ^{12}C and ^{28}Si targets for the second running period. The solid curve is calculated by using the Klein-Nishina formula and adding the $\mathcal{O}(\alpha)$ radiative corrections shown in Fig. 2. The inner error bars are systematic uncertainties and the outer error bars are statistical uncertainties.

distributions. The geometrical acceptance uncertainty was estimated from the variation in the simulated yields with small changes to the experimental geometry. The target thickness uncertainty was 0.05% for the 5% radiation length ^{12}C target. The uncertainty was higher for the thicker targets used during the second running period: 0.11% for the 8% radiation length ^{12}C target and 0.35% for the 10% radiation length ^{28}Si target.

	Running Period	
	I	**II**
Source Of Uncertainty	**^{12}C**	**^{12}C (^{28}Si)**
photon flux	1.0%	0.82%
target composition, thickness	0.05%	0.05 (0.35)%
coincidence timing	0.05%	0.07 (0.22)%
coplanarity	0.078%	0.17 (0.51)%
radiative tail	0.045%	0.045%
geometrical acceptance	0.60%	0.25%
background subtraction	0.72%	0.17 (0.59)%
HyCal energy response	0.50%	0.5%
total	1.50%	1.22 (1.79)%

TABLE I: Estimated systematic errors for each data point.

VI. CONCLUSION

In conclusion, the total cross section for Compton scattering on ^{12}C and ^{28}Si, in the 4.40 - 5.45 GeV energy range was measured with the *PrimEx* experimental apparatus. The results are in excellent agreement with theoretical prediction with NLO radiative corrections. Averaged over all data points per target, the total uncertainties were 1.7% for the first running period, and 1.3%, 1.5%, and 2.5% for the second running period (for 5%

and 8% ^{12}C, and ^{28}Si targets, respectively - see Table I). This measurement provides an important verification of the magnitude and the sign of the radiative effects in the Compton scattering, which determined and separated from the leading order process for the first time. We conclude that the QED next-to-leading order prediction correctly describes this fundamental process up to a few GeV energy within our experimental accuracy.

VII. ACKNOWLEDGEMENTS

This work was funded by the U.S. Department of Energy, including contract #AC05-06OR23177 under which Jefferson Science Associates, LLC operates Thomas Jefferson National Accelerator Facility, and by the U.S. National Science Foundation. We wish to thank the staff of Jefferson Lab for their vital support throughout the experiment.

[1] O. Klein and Y. Nishina, *Z. Phys.*, **52**, 853 (1929).
[2] I. Tamm, *Z. Phys.*, **62**, 545 (1930).
[3] I.M. Brown and R.P. Feynaman, *Phys. Rev.*, **85**, 231(1952).
[4] F. Mandl and T.H.R. Skyrme, *Proc. R. Soc. London*, **A215**, 497 (1952).
[5] Till B. Anders, *Nucl. Phys.*, **87**, 721 (1967).
[6] K.J. Mork, *Phys. Rev.*, **A4**, 917 (1971).
[7] A. Tkabladze, M. Konchatnyi, and Y. Prok, PrimEx Note 42, `http://www.jlab.org/primex/`.
[8] S. Kawabata, Computer Physics Communications, 88, 309 (1995).
[9] Mykhailo Konchatnyi, PrimEx Note 37, `http://www.jlab.org/primex/`.
[10] P. Martel et al., Nucl. Instrum. Meth. A **612**, 46 (2009)
[11] M. Ram and P.Y. Wang, *Phys. Rev. Lett.*, **26**, 476 (1971); *ibid.* **26**, 1210(E)(1971).
[12] F. H. Coensgen, University of California Radiation Laboratory Report UCRL-2413, 1953 (unpublished).
[13] L. V. Kurnosova et al., *Zh. Eksp. Theor. Fiz.*, **30**, 690 (1956) [Sov. Phys. - JETP 3, 546 (1956)].
[14] J. D. Anderson et. al., *Phys. Rev.*, **102**, 1626 (1956).
[15] B. Gittelman et. al., *Phys. Rev.*, **171**, 1388 (1968).
[16] A.T. Goshaw et. al.,*Phys. Rev.*, **D18**, 1351 (1978).
[17] M. Peskin and D. Schroeder, *An Introduction to Quantum Field Theory*, Addison-Wesley Publishing Company (1995).
[18] R. Barlow, Computer Physics Communications, 77, 219 (1993).